Ceramics-Silikáty 69 (2), 263-274 (2025)
www.ceramics-silikaty.cz doi: 10.13168/cs.2025.0011

PREPARATION AND HYDRATION OF SYNTHETIC IRON BEARING YE'ELIMITE DOPED WITH P_2O_5 AND MgO

XUECHENG WANG, ZIXU ZHANG, JINBANG WANG, JIANG ZHU, ZHEN LI, PENG DU, #YONGBO HUANG

Shandong Provincial Key Laboratory of Preparation and Measurement of Building Materials, University of Jinan, Jinan 250022, China

#E-mail: mse_huangyb@ujn.edu.cn

Submitted November 13, 2024, accepted February 20, 2025

Keywords: Sulfur (iron) aluminate cement, Hydration, Phosphorus, Magnesium

In order to enhance the calcination and hydration characteristics of iron bearing ye'elimite (FY), synthetic $C_4A_{2.9}F_{0.1}\$$ was prepared under different temperatures with varying amounts of phosphorus (P_2O_5), magnesium (MgO), and a combination of P_2O_5 and MgO, to investigate early hydration behaviour. The results demonstrate that the formation of FY doped with P_2O_5 at 1200 °C is significantly enhanced, with an increase in hydration observed for 0.5 mass % P_2O_5 compared to 0.25 mass % P_2O_5. At 1250 °C, the FY primarily consists of FR as the major phase, along with a small amount of remaining anhydrite. However, the presence of anhydrite decreases when doped with P_2O_5, disappearing completely at 1300 °C. Without any gypsum present, the FY doped with P_2O_5 exhibits higher hydration activity than pure FY alone. On the other hand, FY doped with MgO shows a broadened main peak within 24 hours, but a lower hydration activity compared to the pure FY alone. Although gypsum accelerates uniform hydration, doping with P_2O_5 still promotes the hydration activity while doping FY with M hinders the broadening range characteristics and reduces the overall hydration activity.

INTRODUCTION

Environmentally friendly cement has gained significant attention in pursuing sustainable development through energy conservation and waste reduction. Calcium sulfoaluminate (CSA) cement is a promising candidate due to its potential benefits [1, 2]. However, the production of Portland cement has led to severe environmental consequences with approximately 0.87 tonnes of CO_2 emissions per tonne of cement produced [3-5]. To address this issue, (ferritic-bearing) calcium sulfoaluminate (FR-CSA) cement has been introduced as an alternative to CSA cement by replacing aluminium with iron and reducing the bauxite costs [6]. The main mineral phase in FR-CSA cement is ferritic bearing ye'elimite ($C_4A_{2.9}F_{0.1}\$$ in cementitious notation where C = CaO, A = Al_2O_3, F = Fe_2O_3, \$ = SO_3), which exhibits different calcination temperatures and hydration specifications that can be optimised for the higher content of ferric-rich calcium sulfoaluminate [7].

Due to the diverse amount of iron added, the target phase of $C_4A_{3-x}F_x\$$ was successfully synthesised by stoichiometrically replacing aluminium with iron. Yao et al. [6] reported that the maximum content in the subscripts, denoted as x in $C_4A_{3-x}F_x\$$, was 0.33, representing the 16.18 wt. % incorporation of Fe_2O_3 and sintered using chemical reagents. Interestingly, Huang et al. [8] prepared iron-rich CSA cement without bauxite by partially substituting Al with waste solid materials, enabling the preparation of iron-rich CSA cement with a distinct raw material composition relative to the mineral phases. Wu et al. [7] further reported that a lower amount of iron was found to be beneficial for gypsum decomposition, while ye'elimite containing a low-iron content and anhydrite exhibited improved results as a liquid phase upgrade for anhydrite dissolution [6, 7]. However, the synthetic ye'elimite exhibits various polymorphs, including orthorhombic and cubic forms [9]. Moreover, it is the presence of iron in the solid solution that induces the transformation from an orthorhombic crystal structure to a pseudo-cubic one, thereby accelerating the hydration process of ferritic-bearing ye'elimite [10]. Despite larger crystal sizes compared to pure ye'elimite, emphasis should still be placed on faster hydration rates [11]. Consistent with previous investigations, a higher iron content in the raw material leads to greater substitution of Fe^{3+} for Al^{3+} in the prepared IR-CSA cement [8]. Additionally, rather than forming a ferrous phase, iron prefers replacing aluminium as it provides a suitable foundation.

In order to achieve a higher yield of ye'elimite at lower temperatures, extensive research has been conducted on the introduction of mineralisers and their effects. The addition of phosphorus (P_2O_5) and

fluorine (F) has demonstrated the ability to decrease the calcination temperature for the preparation of a belite-calcium sulfoaluminate clinker [12, 13]. Previous investigations have shown that P_2O_5 in Portland cement stabilises C_2S and inhibits the formation of C3S [13]. Subsequently, attention has shifted towards investigating CSA cement with the addition of P alone. It has been reported that impurities such as P and F can enable synthesis of ye'elimite at 1200 oC with a reduction in temperature by 100 °C [14]. The presence of P and F stabilises the increased content of C_4A_3\$-c at the expense of C_4A_3\$-o [12,15]. Therefore, introducing P_2O_5 not only promotes ye'elimite formation, but also enhances the content of C_4A_3\$-c. However, due to the prolonged reaction time requirements, the amount of added P_2O_5 cannot be excessively high [16]. This study will discuss incorporating P_2O_5 into $C_4A_{2.9}F_{0.1}$\$, which serves as a foundation for ye'elimite.

As indicated by previous investigations, the presence of MgO positively impacts the activity of raw materials during calcination [16, 17]. This is attributed to the ability of MgO to flux in both liquid and clinker minerals, refining the activity of raw materials and promoting clinker formation [18-21]. Additionally, when MgO is mixed with the raw materials, it increases the liquid content and reduces the viscosity, thereby enhancing the formation of C_4A_3\$ and C_3\$. However, it should be noted that MgO exhibits distinct characteristics when added in small amounts. Therefore, careful control over its addition is necessary to prevent excessive free periclase (more than 5 %), which can compromise the cement soundness. The presence of free periclase has a limiting effect on both Portland and CSA cement. Similar to P's influence, it is essential to investigate solely the impact of MgO in FY. Previous studies have reported that magnesium ions can replace calcium ions in C3S, C_2S, and C_3A [22]. Due to its smaller radius compared to Ca^{2+}, Mg^{2+} can also enter ye'elimite's crystal lattice and induce lattice distortion [17], although this detrimental effect is hindered by the SO_3 presence [23]. Further observation and analysis are required regarding the hydration characteristics and effects on the calcinated mineral phases associated with the added MgO.

The hydration of ye'elimite plays a crucial role in CSA cement, influencing both the setting time and strength development. When iron is added to prepare FY, the calorimetric study reveals lower cumulative heat compared to pure ye'elimite, indicating a longer induction period for the Fe_2O_3 flux [6,7]. Moreover, as the iron content in the FY increases, the hydration with gypsum decreases and delays the occurrence of two peaks in flow heat [7, 24]. It is noteworthy whether gypsum is present in iron-bearing ye'elimite. D·Jansen et al. [25] reported that when gypsum is present, two distinct peaks of heat flow can be observed during the hydration of ye'elimite and iron-containing ye'elimite; however, without gypsum only one peak of heat flow can be detected. This verifies that the hydration reaction of iron-bearing ye'elimite is slower than that of conventional ye'elimite when gypsum is present [24, 26]. Nevertheless, with the addition of P_2O_5 causing distortion in the crystal lattice of ye'elimite, it enhances its hydration reaction; however it also prolongs the setting time compared to synthesised ye'elimite [14].

Moreover, the preparation of a solid solution of $C_4A_{2.9}F_{0.1}$\$ requires careful consideration of the sintering temperatures, particularly in relation to the appropriate mineraliser content. However, these papers lack a comprehensive description of the introduction of P_2O_5, MgO and their coexistence in ferritic-bearing ye'elimite. Therefore, this study aims to synthesise FY doped with MgO and P_2O_5 at different temperatures while ensuring proper amounts are used. Additionally, the synthesised samples will be characterised within 24 h both with and without the presence of gypsum.

EXPERIMENTAL

Materials

The analytical reagents ($CaCO_3$, $CaSO_4·2H_2O$, Al_2O_3, Fe_2O_3, $Ca_3(PO_4)_2$, and MgO) provided by Sinopharm Chemical Reagent Co., Ltd. were utilised to prepare the raw materials. The chemical reagents were accurately weighed for the stoichiometric design of $C_4A_{2.9}F_{0.1}$\$ in order to obtain the mixtures. Among the raw materials, $CaCO_3$ and $CaSO_4·2H_2O$ served as the primary sources of CaO; additionally, P_2O_5 was introduced from $Ca_3(PO_4)_2$ as a supplementary source of calculated CaO to maintain the constant overall composition. This aforementioned addition was divided into six categories: 0.25 mass % P_2O_5, 0.5 mass % P_2O_5, 0.5 mass % MgO, 1.0 mass % MgO, 0.25 mass % P_2O_5 + 0.5 mass % MgO, and 0.5 mass % P_2O_5 + 1.0 mass % MgO added into the mixtures accordingly. Table 1 presents the proportions of these raw materials.

The mixtures were then homogenized and combined with 10 wt. % water before being shaped into discs under a pressure of 10 MPa. Subsequently, the cement raw meal discs were dried in an oven at 65 °C for 24 h and placed individually in alundum crucibles without overlapping. Finally, the samples were sintered separately at temperatures of 1050 °C, 1100 °C, 1150 °C, 1200 °C, 1250 °C, and 1300 °C (with a heating rate of 5 °C·min^{-1} from room temperature to the desired temperature) for two hours, followed by rapid cooling to the ambient air or room temperature. The hydration process was investigated by incorporating sufficient gypsum into the synthetic (FY, FY-0.5P, FY-1.0M, FY-0.5P-1.0M) powder to explore its reaction with a water-to-cement ratio (w/c) of 0.5.

Table 1. Proportions of the raw materials of the synthetic C4A2.9F0.1$ (g).

Sample	$CaCO_3$	Al_2O_3	Fe_2O_3	$CaSO_4$	$Ca_3(PO_4)_2$/MgO
FY	48.62	47.89	2.59	22.04	-
FY-0.25P	48.09	47.89	2.59	22.04	0.546/0
FY-0.5P	47.56	47.89	2.59	22.04	1.093/0
FY-0.5M	48.62	47.89	2.59	22.04	0/0.5
FY-1.0M	48.62	47.89	2.59	22.04	0/1.0
FY-0.25P-0.5M	48.09	47.89	2.59	22.04	0.546/0.5
FY-0.5P-1.0M	47.56	47.89	2.59	22.04	1.093/1.0

FY-B stands for pure $C_4A_{2.9}F_{0.1}$. FY-0.25P and FY-0.5P stands for $C_4A_{2.9}F_{0.1}$ doped with 0.25 % P_2O_5 and 0.5 % P_2O_5, differently. FY-0.5M and FY-1.0M stands for $C_4A_{2.9}F_{0.1}$ doped with 0.5 % MgO and 1.0 % MgO, respectively. FY-0.25P-0.5M and FY-0.5P-1.0M stands for $C_4A_{2.9}F_{0.1}$ doped with 0.25 % P_2O_5 and 0.5 % MgO and 0.5 % P_2O_5 and 1.0 % MgO, separately.

Methods

Laboratory X-ray powder diffraction (XRD) measurement

After necessary milling, the powder was applied to the XRD analysis on a D8 Advance diffractometer, Germany, using CuKα radiation at 40 kV and 40 mA. It was applied for continuous rotation during the data acquisition. The range of 5°-65° with a step size of 0.02° to acquire a content result of the quantitative phase analysis, while an overall measurement time of 2 h per pattern was required for great statistics. The hydration of the specimens was stopped with acetone, followed with diethyl ether to remove the free water and then stored in a desiccator over gel lime (to ensure the protection against the H_2O and CO_2) for the above-stated XRD analysis [27].

Rietveld quantitative phase analysis (RQPA)

The samples were supplied for the quantitative analysis by the TOPAS-academic software as the Rietveld methodology. The replacement of Al^{3+} to Fe^{3+} as the stoichiometric $C_4A_{2.9}F_{0.1}$ was in good promotion to the solid solution, improving the complexity of the Rietveld analysis [7, 28]. Therefore, the refinement for minimising the common problems including peak overlapping, preferred orientation and solid solutions was adopted to fit the complete profile and background and requires the knowledge of the overall crystal structure [29]. The crystallographic structures, shown in Table 2, are used for the refinement of the samples.

Table 2. Crystallographic structures used in the Rietveld quantitative phase analysis.

Phase	Space group	ICSD code
C_4A_3-o	14-3m	80.361
C_4A_3-c	Pcc2	9560
C_4AF	Pcmn	9197
C$	Amma	1956
C	Fm3m	52.783
$C_{12}A_7$	143d	241.003
M	Fd3m	

Scanning electron microscopy (SEM)

The fractured surface of the samples was coated with Au in a vacuum to satisfy the conductivity requirement. A TESCAN VEGA 3 was applied for the SEM analysis at a voltage of 5 kV and a current of 20 μA.

Isothermal conduction calorimetry

The heat release of $C_4A_{2.9}F_{0.1}$ was recorded with an eight channel TAM AIR colorimeter. The measurement was conducted on the sample with a w/c of 0.5. After putting the electric agitator loaded with a sample and water into the chamber. Twelve hours were needed for the system to reach equilibrium. Then the sample was mixed with water and stirred by the electric agitator for 2 min. The measurement lasted for 24 h at a constant temperature of 20 °C.

The solution analyses of sample treatment by ICP-OES

Arriving at punctual time of the scheme, the appropriate range of solution from 10 to 15 ml was taken, filtered with 0.45 μm nylon filters. As soon as the filtration finished, the continuous measurement of conductivity and pH was carried out to supply the data in time with the untreated solution. In order to avoid precipitation, the samples were acidified with 65 % HNO_3 and the difference with and without HNO_3 was measured with identical results in the previous investigation [30, 31]. The measurement of the solution composition tested for Al, Ca, K, Na, S, and Si (ICP-OES, Varian Vista Pro with a CCD-detector) within 24 h. The limit of detection should be satisfied with a dilution below 0.01 mmol·L^{-1} [31].

RESULTS AND DISCUSSION

Characterisation of the synthetic FR-Y

The XRD pattern of the mineral phase sintered at temperatures ranging from 1050 °C to 1300 °C for 2 h is

presented in Figure 1. At 1050 °C, the main diffraction peaks correspond to $CaSO_4$ and CaO, with intermediate phases including $CaAl_2O_4$, $Ca_3Al_2O_6$, $Ca_{12}Al_{14}O_{33}$, and weak diffraction peaks of $C_4A_{2.9}F_{0.1}$\$. As the temperature increases, a slight increase in the intensity of the $C_4A_{2.9}F_{0.1}$\$ peak is observed at 1100 °C. At 1150 oC, enhanced formation of $C_4A_{2.9}F_{0.1}$\$ accompanied by a decrease in the diffraction intensity of $CaSO_4$ can be seen. The intensive enhancement of the $C_4A_{2.9}F_{0.1}$\$ peak doped with P_2O_5 is observed at 1200 °C; conversely, both $CaSO_4$ and CaO show decreased intensities as well. Previous studies have reported that phosphogypsum decomposition for ye'elimite preparation exhibits promotion at 1200 °C [32,33]. Furthermore, the presence of Fe_2O_3 enhances the decomposition of $CaSO_4$ [34]. In comparison to the inconspicuous intensity peak observed for MgO added and referred FY, it can be concluded that P_2O_5 promotes the decomposition of anhydrite. At 1250 °C, there is a significant decrease in the peak intensity of $CaSO_4$, resulting in the formation of $C_4A_{2.9}F_{0.1}$\$ and nearly disappearing diffraction peaks for CaO. The reduced diffraction peak mentioned above highlights a higher concentration of $C_4A_{2.9}F_{0.1}$\$ laterally. Upon reaching 1300 °C and the complete disappearance of C\$, the dominant intensity peak corresponds to $C_4A_{2.9}F_{0.1}$\$, with only a small amount of intermediate phases present, which is crucial for further hydration studies.

Table 3 shows the content of the phase assemblage in the samples sintered at 1300 °C for four hours. In greater detail it is more effectively performed through the visual data of Rietveld analysis. As previously investigated, an Rwp account of less than 10 % highly validates the reliability. However, in the qualitative results for TC_4A_3\$, the weight ratio implies little difference due to the nearly identical content. C_4A_3\$ has two polymorphs: orthorhombic and cubic [9], which require separate analysis to distinguish samples doped with P_2O_5, MgO, or both. Consequently, when comparing FY values, FY-0.5P promotes the higher content of C_4A_3\$-c at the expense of C_4A_3\$-c for the approximate TC_4A_3\$.

Additionally, these findings align with previous investigations demonstrating that sufficient time can increase the formation of C_4A_3\$ [16]. Similarly, the results characterise the content of C_4A_3\$-c in samples doped with P_2O_5, MgO, and a combination of P_2O_5 and

Table 3. Phase assemblage content of the samples at 1300 °C for 4 h (wt. %).

Mineral	C_4A_3\$		C_4AF	$CaSO_4$	CaO	$Ca_{12}Al_{14}O_{33}$	MgO	TC_4A_3\$	Rwp
	C_4A_3\$-o	C_4A_3\$-c							
FY	77.3	17.9	1.7	0.4	0.9	1.8	0	95.2	8.23
FY-0.5P	74.3	22.1	1.6	0.2	0.6	1.2	0	96.4	7.98
FY-1.0M	71.0	24.1	2.1	0.3	0.7	1.1	0.7	95.1	7.69
FY-0.5P-1.0M	69.5	26.8	1.4	0.3	0.5	1.0	0.5	96.3	8.40

o: orthorhombic, c: cubic TC_4A_3\$: the total calculation both the orthorhombic and cubic C_4A_3\$

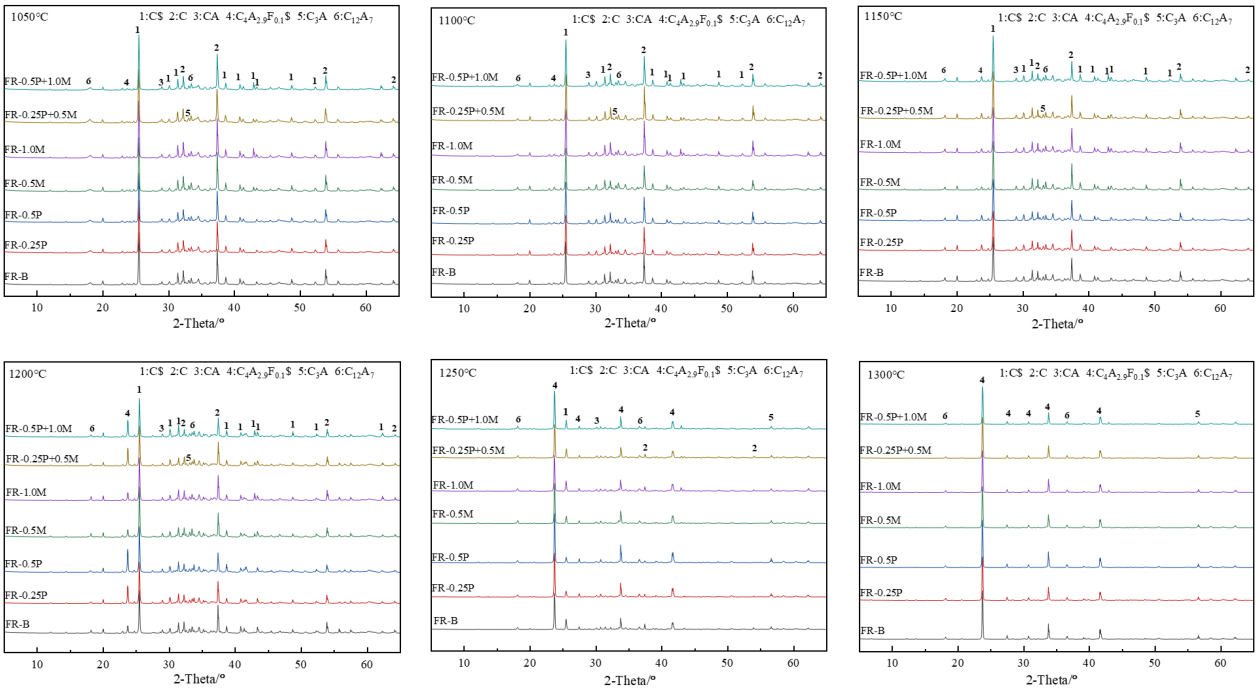

Figure 1. XRD patterns of the specified temperatures.

MgO. It is noteworthy that the sample doped with the coexistence of P_2O_5 and MgO exhibits an even higher content of C_4A_3\$-c. Interestingly, the addition of P_2O_5 stabilises lime to form C_4A_3\$, while the coexistence of MgO and P_2O_5 further enhances this effect. The content of C_4AF should be given attention as in previous investigations [17]. However, instead of displacing Ca^{2+} or entering the crystal lattice, a higher content of free MgO is detected compared to the introduction of P2O5 in FY-0.5P-1.0M. Therefore, it is hypothesised that the coexistence of MgO and P_2O_5 contributes to the stabilisation of MgO through the favourable exsolution of sulfate [35].

Additionally, lime not only participates in the formation of C_4A_3\$, an intermediate phase of $C_{12}A_7$ resulting from the decomposition of C_4A_3\$, but its content also serves as evidence for thermal stability. It has been reported that the decomposition of C_4A_3\$ occurs when temperatures exceed 1300 °C [36]. Consequently, mineralisers such as MgO and P_2O_5, and their coexistence refine the thermal stability of FY.

The SEM photographs of the samples calcined at 1300 °C for four hours are presented in Figure 2. FY exhibits a partial solid solution formation due to the fluxing effect of iron. Previous investigations have reported that Fe^{3+} (r = 0.069 nm) has a larger radius than Al^{3+} (r = 0.053 nm), resulting in Fe^{3+} occupying the octahedral position in the phase structure, which differs from Al^{3+} locating at the tetrahedral position [6]. In FY-0.5P, the addition of 0.5 mass % P_2O_5 into the sample results in the presence of the $C_4A_{2.9}F_{0.1}$\$ mineral phase with enhanced adhesive crystal boundaries. The crystal particles exhibit an increased size compared to FY, surpassing 2 μm and hindering the hydration reactivity. In FY-1.0M, it is observed that the inclusion of 1.0 mass % MgO promotes the formation of smaller particles with free MgO adhering to their surfaces, consistent with Table 3's findings for MgO samples. Additionally, it can be noted that samples containing 1.0 mass % MgO exhibit greater compactness due to firing shrinkage as reported in a previous study [16]. For FY-0.5P-1.0M, homogenised particle sizes around 2 μm are observed along with a more orderly shape and compact arrangement of crystal particles.

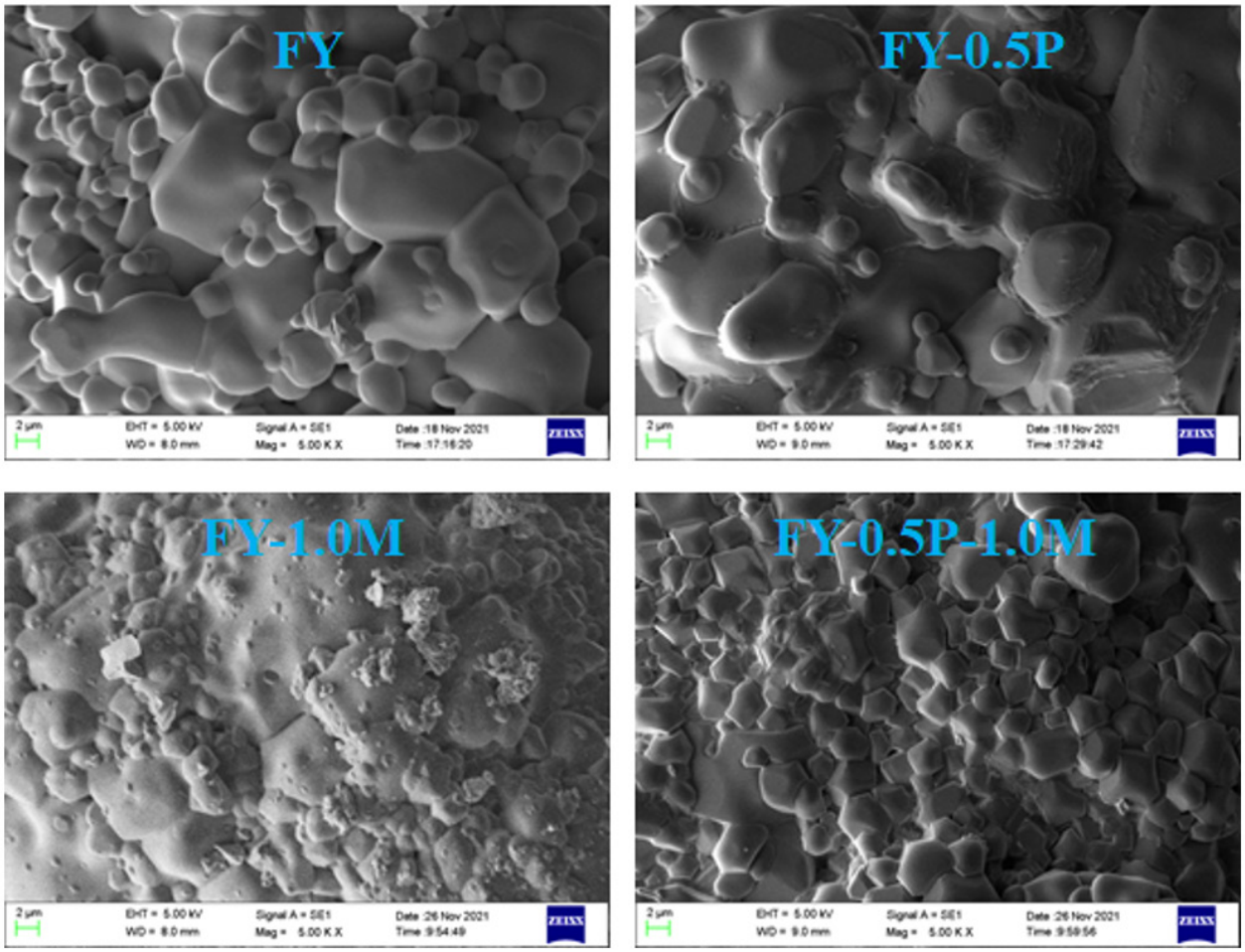

Figure 2. The SEM photographs of synthetic $C_4A_{2.9}F_{0.1}$\$ with the calcination at 1350 °C for 4 h.

Early-age hydration of synthetic FY

The hydration characteristics of the synthetic samples were investigated using isothermal conduction calorimetry measurements. Figure 3 illustrates the heat flow of the samples in the absence of gypsum. The initial heat release within the first 0-0.2 h can be attributed to the wetting of the system, partial dissolution of gypsum and ye'elimite, and formation of initial hydrates (AFm/AFt and AH_3) [25, 37-39]. In the presence of gypsum, dissolution occurs within a range extending up to 0.4 hours during this initial period. Additionally, it has been reported that iron-bearing ye'elimite exhibits higher hydration activity compared to pure ye'elimite with similar hydration sequence and products; however, its induction period is prolonged [40-42].

After an initial period, the heat flow curve of the sample FY can be characterised by two minor exothermic peaks and one prominent peak. The first minor peak reaches its maximum at 1.8 h with a heat flow of 3.25 $mW \cdot g^{-1}$. The specific characteristics of this observed peak remain unclear, possibly associated with pure ye'elimite. Following the first weak peak is a second weak peak that exhibits faster reactivity compared to FY-0.5P, FY-1.0M, and FY-0.5P-1.0M, aligning well with $C_{12}A_7$ [31]. This second minor peak reaches its maximum at 3.8 h with a heat flow of 2.70 $mW \cdot g^{-1}$. The subsequent exothermic peak reaches its maximum at 8.8 h with a heat flow of 15.4 $mW \cdot g^{-1}$. In addition, as previously reported [43], the total hydration heat decreases accordingly. After reaching its summit point, the main peak gradually diminishes without any shoulder until 24 h.

The heat flow of sample FY, with the addition of 0.5 mass % P_2O_5, is characterised by one weak peak and one steep peak as the main reaction of high hydration activity. However, when compared to FY-0.5P, it is demonstrated that the substitution of $[PO_4]$ (rp^{5+} = 38 ppm) for $[SO_4]$ (rs^{6+} = 29 ppm) results in an increased d value [44]. As shown in Figure 2, a more fluxed solid solution is observed and the enlarged d value hinders the hydration. Previous investigations have also reported that adding a suitable amount of P_2O_5 increases the hydration activity of $C_4A_3\$$ [13]. Therefore, the substitution of $[SO_4]$ with $[PO_4]$ induces lattice distortion in P_2O_5, thereby enhancing its hydration activity. It has also been reported that the addition of phosphorus slightly increases $C_4A_3\$$-c at the expense of $C_4A_3\$$-o [45, 46]. The steep peak summit of FY-0.5P at 9.2 h, reaching a maximum value of 37.9 $mW \cdot g^{-1}$, occurs later than that of FY, but exhibits higher hydration activity. Corresponding to this active hydration process, the total cumulative value at 24 h is significantly increased. Simultaneously, there is a rapid decrease in the steep peak with a narrower range compared to FY.

The heat flow of FY-1.0M is characterised by a broad peak starting at 5.0 h and a weaker one, with the maximum heat flow of 13.6 $mW \cdot g^{-1}$ occurring at 11.9 h, slightly lower than that of FY. Despite the distortion caused by the Mg ion incorporation into the crystal lattice of $C_4A_3\$$, the hydration and calcination processes lead to the exsolution of MgO influenced by SO_3, resulting in a non-negligible free MgO content. Previous studies have reported that Mg can form not only substitutional, but also interstitial solid solutions within cement clinkers [47]. Revised sentence: Regardless of whether Mg^{2+} is replaced by Ca^{2+}, the interstitial atom, or even free MgO, delayed hydration occurs in the absence of gypsum. In Figure 4, FY-1.0M demonstrates lower reactivity, but a wider range of reaction during hydration. It can be easily observed that FY-1.0M exhibits higher cumulative heat compared to FY. After 20 h, the heat flow curve shows a higher heat flow rate than that of FY. The weak peak preceding the sharp peak in FY-1.0M indicates a delay similar to that observed in FY and lower hydration

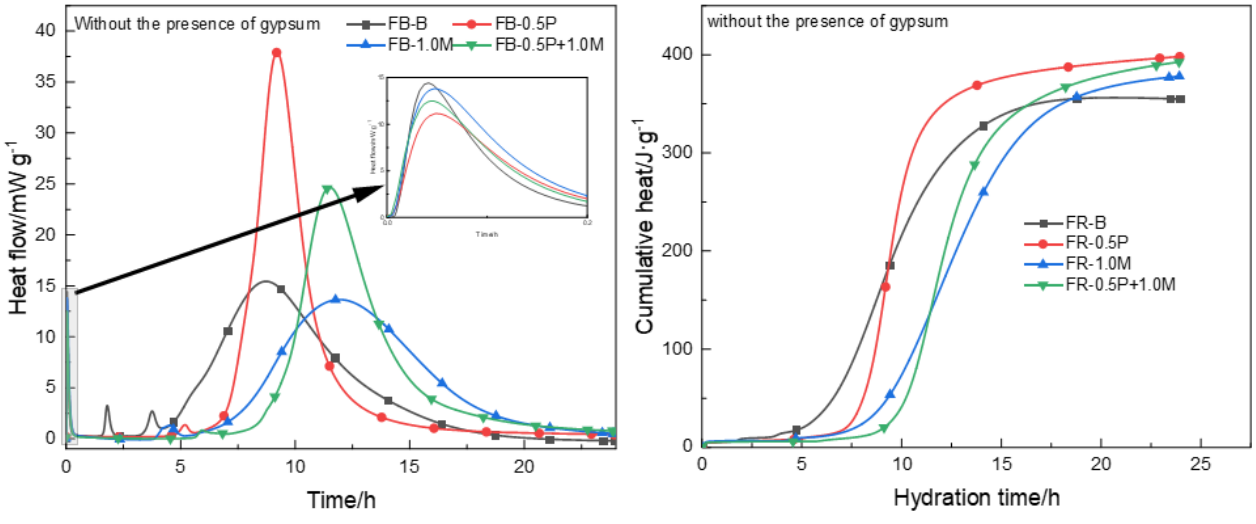

Figure 3. Heat flow without the presence of gypsum in the different samples.

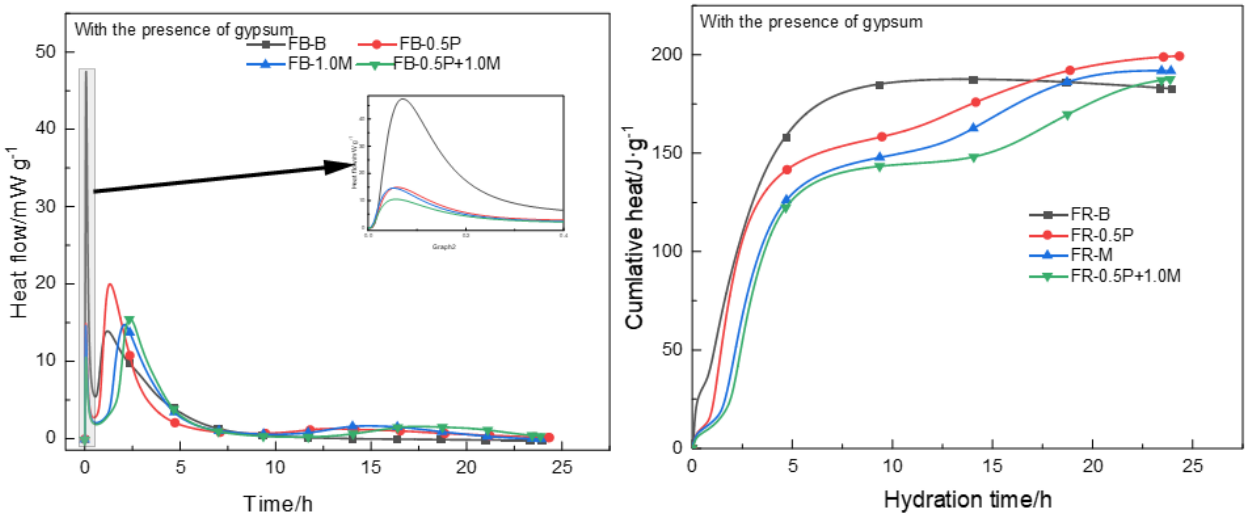

Figure 4. Heat flow with the presence of gypsum in the different samples.

activity. The limited presence of FY-1.0M in Figure 2 reveals the emergence of free periclase on the surface of the solid solution, although its impact on the hydration is considered minimal. The incorporation of MgO distorts the lattice structure of $C_4A_{2.9}F_{0.1}$\$ and enhances the fluxing phase due to its low solubility when added in small quantities. Consequently, substituting Ca^{2+} for Mg^{2+} and occupying the lattice sites of $C_4A_{2.9}F_{0.1}$\$ significantly influences the hydration by delaying the primary reaction and extending its duration.

The heat flow curve of sample FY-0.5P-1.0M exhibits a distinct peak and an emphasised peak, demonstrating hysteresis as the weak peak reaches its maximum at 5.9 h with a magnitude of 0.8 $mW \cdot g^{-1}$. The presence of both MgO and P_2O_5 causes a delay in the occurrence of the weak peak compared to individual samples FY, FY-0.5P, or FY-1.0M without gypsum present as described earlier. Furthermore, the summit of the weak peak is lower than that observed for FY doped solely with MgO or P_2O_5. The joint effect of coexistence of P_2O_5 and MgO doping is manifested in the subsequent steep peak, which exhibits higher reactivity compared to FY, but lower than FY-0.5P with a similar shape of heat flow peak. Referring to Table 2, both Mg as the replacement atom and interstitial atom decrease hydration reactivity, although unreacted free periclase still dominates. In contrast to FY-0.5P, the wider range of the highlighted peak is primarily associated with FY-1.0M. The highlighted peak of FY-1.0M reaches its maximum at 11.9 h, while that of FY-0.5P-1.0M nearly coincides with it at 11.5 h with a slightly earlier maximum value of 24.6 $mW \cdot g^{-1}$. Moreover, the incorporation of MgO and P_2O_5 demonstrates a joint effect on shaping the main peak profile predominantly through the addition of P_2O_5. According to Table 3, one of the quantitative advantages of MgO is attributed to its higher amount of C4A3$-c. The improved hydration activity and broadened width of the highlighted peak result in an indistinctive cumulative heat at 24 h for FY-0.5P-1.0M compared to FY-0.5P alone. Previous investigations have shown that the addition of MgO leads to an increase in the cumulative heat [48]. A similar consequence is observed with the addition of 1.0 wt. % MgO. Therefore, the coexistence of MgO and P_2O_5 introduces a comparable comprehensive influence.

The hydration of samples in the presence of gypsum is illustrated in Figure 5. Previous studies have reported that the addition of gypsum leads to a more uniform hydration development [47, 49]. However, further investigation is required to explore the effects

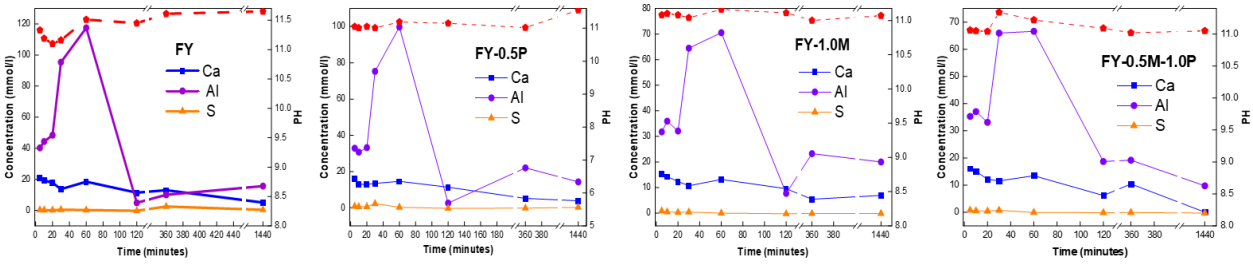

Figure 5. The evolution solution composition without the presence of gypsum.

of introducing MgO, P_2O_5, and their coexistence. The introduction of gypsum enables the detection of two distinct heat flow maxima during the ye'elimite hydration, as previously investigated [25, 50-52]. The second peak appears delayed and reduced following the initial steep peak, possibly due to iron-bearing compounds. In the presence of an adequate sulfur source, ettringite formation is accelerated along with highly hydrated AH_3.

After an initial period, the occurrence of FY still precedes in the presence of gypsum during the range of the first steep peak. The wide range of this steep peak is clearly evident, while the second peak of FY appears to be relatively flat. It can be concluded that the second peak becomes trapped at the end of the first steep peak due to its lower hydration activity.

The heat flow of FY-0.5P exhibits higher reactivity in the main steep peak compared to FY, indicating enhanced hydration. The delayed setting is partially compensated by the presence of gypsum. The distance between the summit of the first peak for FY and FY-0.5P decreases significantly, as well as its onset. Therefore, the introduction of P in FY increases the amount of $C_4A_{2.9}F_{0.1}$\$-c and also promotes hydration due to the presence of gypsum with an unclarified function.

With sufficient sulfur content, the influence on the broad peak doped with MgO appears to be restrained. The hydration reactivity surpasses that of FY slightly, resulting in an earlier setting compared to FY-0.5P-1.0M. Consequently, the presence of gypsum accelerates the hydration process of FY-1.0M towards FY. The weak peak of FY-1.0M becomes prominent following the peak of FY-0.5P. It has been reported that MgO-doped C_3S broadens the second peak and enhances cumulative heat [47]. Similar tendencies are observed for both the second peak in heat flow and cumulative heat in Figure 6.

Regarding FY-0.5P-1.0M, the initial peak summit is observed to occur later compared to FY-1.0M. Moreover, the broadening range of the primary peak does not exhibit significant similarity in terms of its influence on the FY doped with 1.0 % MgO. Irrespective of the presence or absence of gypsum, it is evident that the coexistence of MgO and P_2O_5 has an observable impact, wherein their combined effect enhances the hydration reactivity during the reaction process. The second peak demonstrates a delayed yet enhanced reaction, thereby highlighting the synergistic influence. Therefore, the introduction period delay of FY-0.5P-1.0M is further enhanced due to the distortion of the $C_4A_{2.9}F_{0.1}$\$ lattice caused by P_2O_5 or MgO doping, both during the delayed introduction period and collectively influencing it, regardless of the presence of gypsum.

The results with different set periods are depicted in Figure 5 and Figure 6, where the red dashed line above the curves of Ca, Al, and S represents the pH. Comparing the pH values between the absence and presence of gypsum, it can be observed from Figure 6 that gypsum promotes a stronger tendency towards hydration. In addition, when gypsum is present during ye'elimite hydration, the second step involving S ions shows a direct correlation with ettringite precipitation powered by the ye'elimite consumption without any dissolution of gypsum as reported previously [25, 53].

The XRD analysis reveals, in Figure 7, that the hydration of $C_4A_{2.9}F_{0.1}$\$ exhibits distinct phases, even in the absence of gypsum. However, when gypsum is present, subtle variations in the hydration and ettringite formation is observed over time. Despite a lower quantity compared to the unreacted anhydrite, the diffraction peaks at 6 h and 1 d with gypsum can be distinguished. In contrast, at 3 d and 7 d, the presence of gypsum disappears while the diffraction peak of ettringite stabilises, indicating a sufficient sulfur source crucial for the $C_4A_{2.9}F_{0.1}$\$ hydration. In contrast, the presence of gypsum leads to the overtaking of the diffraction peaks of ettringite at 6 h compared to the results shown in Figure 7. Furthermore, distinct variations in intensity can be observed for the diffraction peaks when MgO, P_2O_5, or both are added. The samples doped with MgO exhibit a rapid hydration period occurring 1 d to 3 d earlier than those with P_2O_5 and FY, indicating that the smaller size of the M-added powder hinders the hydration as depicted in Figure 2. The FY and FY-0.5P values both fall within the range of 3 d to 7 d. Notably, the diffraction peak intensity of ettringite during early hydration exhibits a similar trend. Consequently, the addition of MgO and P_2O_5 influences the process rather than the outcome of the hydration.

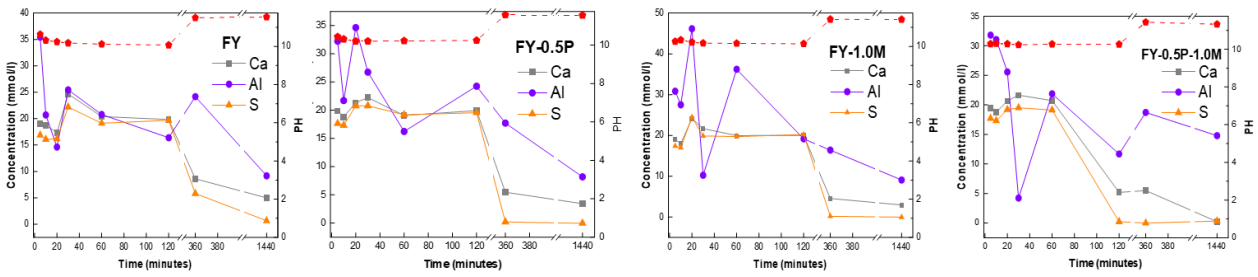

Figure 6. The evolution solution composition with the presence of gypsum.

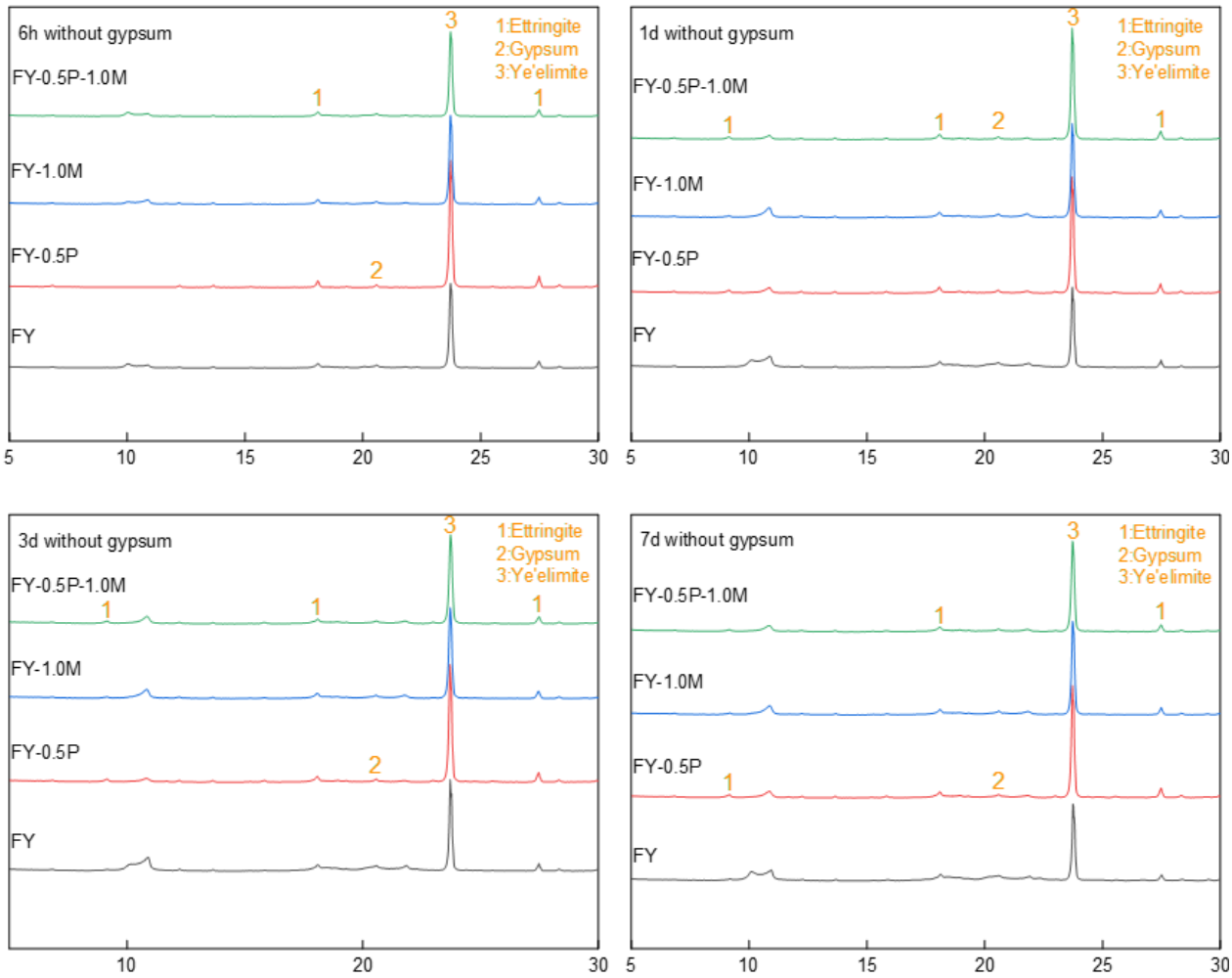

Figure 7. The hydration without the gypsum of $C_4A_{2.9}F_{0.1}\$$.

CONCLUSION

The study yields the following conclusions:

(1) At temperatures of 1050 °C, 1100 °C, and 1150 °C, the formation of FY exhibits similar characteristics to the introduction of P_2O_5 and MgO, as well as their simultaneous presence. However, upon reaching a temperature of 1200 °C, the characteristic samples doped with P_2O_5 significantly enhance the formation of $C_4A_{2.9}F_{0.1}\$$. Subsequently, at 1250 °C, most of the FY has undergone calcination with minimal unreacted $CaSO_4$ remaining and the scarce presence of free lime can be observed. Finally, at 1300 °C, FY becomes the dominant mineral phase except for any interstitial phases.

(2) The quantitative analysis results presented in Table 3 of the RQPA demonstrate that the introduction of P_2O_5, MgO, and their coexistence promotes the formation of $C_4A_3\$$-c at the expense of $C_4A_3\$$-o and stabilised lime. Moreover, it is observed that P_2O_5 can better flux the sample doped with MgO due to the exsolution of sulfurate. These mineralisers enhance thermal stability as indicated by a higher content of remaining mayenite compared to FY.

(3) Without the presence of gypsum, the addition of P_2O_5 to FY enhances its hydration activity and cumulative heat generation compared to the pure FY. Similarly, incorporating MgO into FY results in higher cumulative heat than FB, but slightly lower reactivity than the pure FY, indicating a broadened main peak of hydration at early ages. The combined effect of P_2O_5 and M is depicted in Figure 3 as an extended range of the main peak and enhanced hydration activity compared to the pure FY.

(4) The presence of gypsum enhances the hydration process of FY and synergistically refines it. However, the addition of P_2O_5 to FY significantly increases its hydration activity and effectively mitigates the delayed reaction with gypsum, bringing it closer to that observed in pure FY. On the other hand, the M-doped samples exhibit promoted hydration upon the introduction of gypsum, but display a broader range characteristic and reduced hydration activity. In the synthetic FY, while the

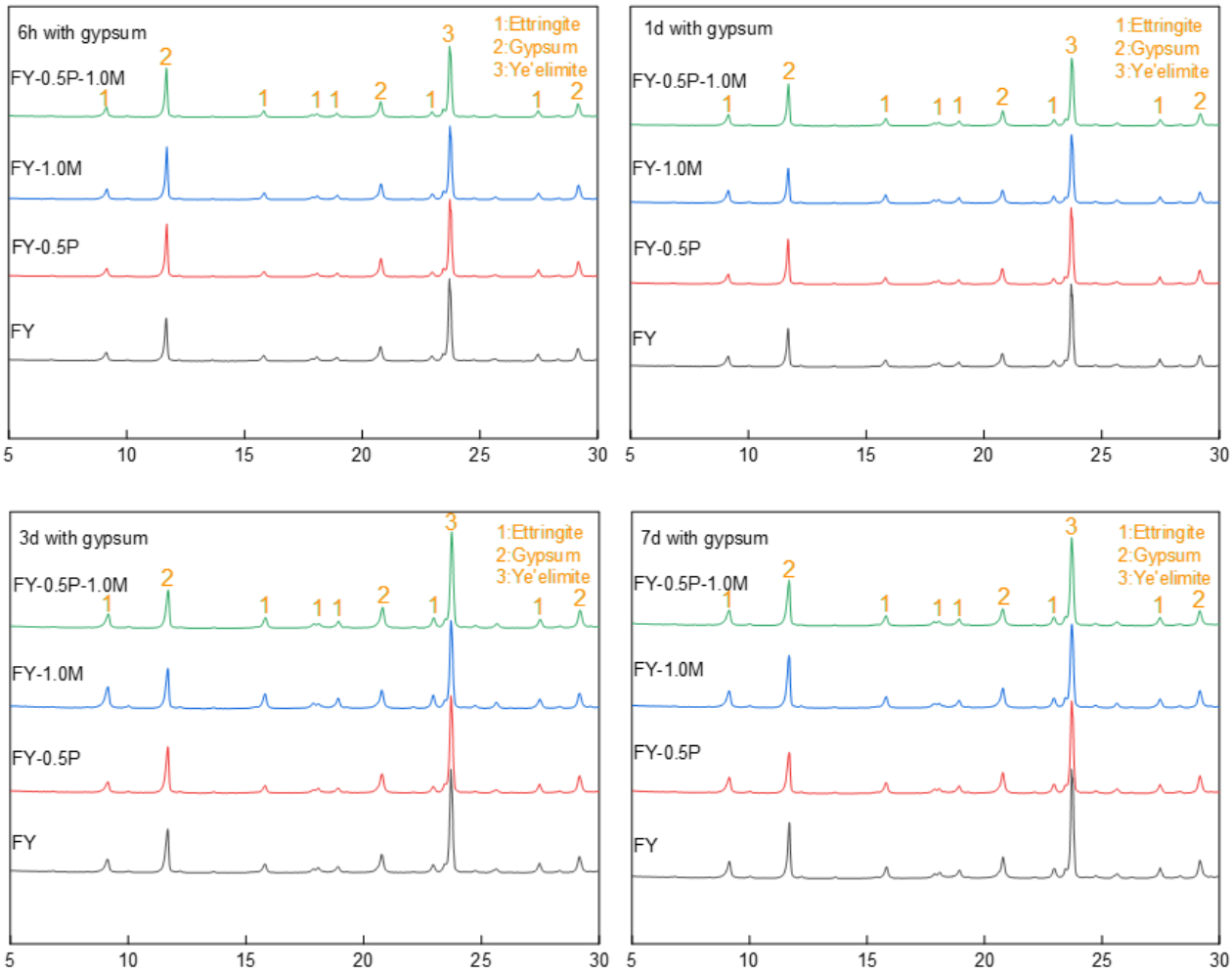

Figure 8. The hydration with the gypsum of $C_4A_{2.9}F_{0.1}\$$.

second peak in hydration remains relatively flat when iron is present, slight doping with P_2O_5 or MgO alters this behaviour slightly.

Acknowledgements

The authors gratefully acknowledge the financial support from National Key Research and Development Program of China (2022YFE0208200), Natural Science Foundation of China (52372027), Natural Science Foundation of Shandong Province (2023TSGC0937), Taishan Scholars Program (tsqnz20221144), Science and Technology project of Inner Mongolia Autonomous Region (2022YFHH0118, 2023YFHH0085, 2023YFHH0086).

REFERENCES

1. Gartner E., Hirao H. (2015): A review of alternative approaches to the reduction of CO_2 emissions associated with the manufacture of the binder phase in concrete. *Cement and Concrete Research, 78*, 126-142. doi:10.1016/j.cemconres.2015.04.012
2. Gartner E. M., Macphee D. E. (2011): A physico-chemical basis for novel cementitious binders. *Cement and Concrete Research, 41*(7), 736-749.doi:10.1016/j.cemconres.2011.03.006
3. Galan I., Elhoweris A., Hanein T., Bannerman M. N., Glasser F. P. (2017): Advances in clinkering technology of calcium sulfoaluminate cement. *Advances in Cement Research, 29*(10), 405-417. doi:10.1680/jadcr.17.00028
4. Huang Y., Qian J., Liu C., Liu N., et al. (2017): Influence of phosphorus impurities on the performances of calcium sulfoaluminate cement. *Construction and Building Materials, 149*, 37-44.doi:10.1016/j.conbuildmat.2017.05.028
5. Zhang P., Li D., Qiao Y., Zhang S., Sun C., Zhao T. (2018): Effect of air entrainment on the mechanical properties, chloride migration, and microstructure of ordinary concrete and fly ash concrete. *Journal of Materials in Civil Engineering, 30*(10), 04018265. doi: 10.1061/(ASCE)MT.1943-5533.0002456
6. Yao X., Yang S., Huang Y., Wu S., Yao Y., Wang W. (2020): Effect of $CaSO_4$ batching in raw material on the iron-bearing mineral transition of ferric-rich sulfoaluminate

cement. *Construction and Building Materials, 250*, 118783. doi:10.1016/j.conbuildmat.2020.118783

7. Wu S., Yao X., Ren C., Yao Y., Zhang C., Wu C., Wang W. (2021): Effect of iron on the preparation of iron-rich calcium sulfoatablluminate cement using gypsum as the sole calcium oxide source and its incorporation into mineral phases. *Construction and Building Materials, 290*, 123214. doi:10.1016/j.conbuildmat.2021.123214
8. Huang Y., Pei Y., Qian J., Gao X., Liang J., et al. (2020): Bauxite free iron rich calcium sulfoaluminate cement: Preparation, hydration and properties. *Construction and Building Materials, 249,* 118774. doi:10.1016/j.conbuildmat.2020.118774
9. Álvarez-Pinazo G., Cuesta A., García-Maté M., Santacruz I., et al. (2012): Rietveld quantitative phase analysis of Yeelimite-containing cements. *Cement and Concrete Research, 42*(7), 960-971. doi: 10.1016/j.cemconres.2012.03.018
10. Bullerjahn F., Scholten T., Scrivener K. L., Haha M. B., Wolter A. (2020): Formation, composition and stability of ye'elimite and iron-bearing solid solutions. *Cement and Concrete Research, 131*, 106009. doi:10.1016/j.cemconres.2020.106009
11. Ndzila J. S., Liu S., Jing G., Wang S., Ye Z. (2020): The effect of Fe^{3+} ion substitution on the crystal structure of ye'elimite. *Ceramics - Silikaty, 64*, 18-28. doi: 10.13168/cs.2019.0044
12. Huang Y., Qian J., Kang X., Yu J., Fan Y., et al. (2019): Belite-calcium sulfoaluminate cement prepared with phosphogypsum: Influence of P_2O_5 and F on the clinker formation and cement performances. *Construction and Building Materials, 203*, 432-442. doi:10.1016/j.conbuildmat.2019.01.112
13. Ifka T., Palou M. T., Bazelova Z. (2012): Influence of CaO and P_2O_5 of bone ash upon the reactivity and the burnability of cement raw mixtures. *Ceramics-Silikáty, 56*(1), 76-84.
14. Huang Y., Qian J., Liang J., Liu N., Li F., Shen Y. (2016): Characterization and calorimetric study of early-age hydration behaviors of synthetic ye'elimite doped with the impurities in phosphogypsum. *Journal of Thermal Analysis and Calorimetry, 123*, 1545-1553.doi: 10.1007/s10973-015-5009-y
15. Huang Y., Qian J., Lu L., Zhang,W., et al. (2020): Phosphogypsum as a component of calcium sulfoaluminate cement: Hazardous elements immobilization, radioactivity and performances. *Journal of Cleaner Production, 248,* 119287. doi:10.1016/j.jclepro.2019.119287
16. Liu X., Li Y., Zhang N. (2002): Influence of MgO on the formation of Ca_3SiO_5 and $3CaO{\cdot}3Al_2O_3{\cdot}CaSO_4$ minerals in alite–sulphoaluminate cement. *Cement and Concrete Research, 32*(7), 1125-1129. doi:10.1016/S0008-8846(02)00751-2
17. Song Q., Su J., Nie J., Li H., et al. (2021): The occurrence of MgO and its influence on properties of clinker and cement: a review. *Construction and Building Materials, 293*, 123494. doi:10.1016/j.conbuildmat.2021.123494
18. Liu G. Q., Yang Q. X., Jiang L., Xue P., et al. (2017): Sintering characteristics of BCSAF cement clinker with added wastes from production of manganese and magnesium metals. *Advances in Cement Research, 29*(6), 227-235. doi:10.1680/jadcr.16.00035
19. Ludwig H. M., Zhang W. (2015): Research review of cement clinker chemistry. *Cement and Concrete Research, 78*, 24-37. doi:10.1016/j.cemconres.2015.05.018
20. Schoon J., Vergari A., De Buysser K., Van Driessche I., De Belie N. (2013): Fines extracted from porphyry and dolomitic limestone aggregates production: MgO as fluxing agent for a sustainable Portland clinker production. *Construction and Building Materials, 43*, 511-522. doi:10.1016/j.conbuildmat.2013.02.046
21. Wang C., Zhou Z., Liu C., Cheng X. (2011): Formation kinetics of portland cement clinker containing with magnesium oxide. *Journal of the Chinese Ceramic Society, 39*(4), 714-717.
22. Zhao R., Zhang L., Fan G., Chen Y., Het al. (2021): Probing the exact form and doping preference of magnesium in ordinary Portland cement clinker phases: A study from experiments and DFT simulations. *Cement and Concrete Research, 144*, 106420. doi:10.1016/j.cemconres.2021.106420
23. Li X., Xu W., Wang S., Tang M., Shen X. (2014): Effect of SO_3 and MgO on Portland cement clinker: Formation of clinker phases and alite polymorphism. *Construction and Building Materials, 58*, 182-192.doi:10.1016/j.conbuildmat.2014.02.029
24. Jansen D., Spies A., Neubauer J., Ectors D., Goetz-Neunhoeffer F. (2017): Studies on the early hydration of two modifications of ye'elimite with gypsum. *Cement and Concrete Research, 91*, 106-116. doi:10.1016/j.cemconres.2016.11.009
25. Jansen D., Spies A., Neubauer J., Ectors D., Goetz-Neunhoeffer F. (2017): Studies on the early hydration of two modifications of ye'elimite with gypsum. *Cement and Concrete Research, 91*, 106-116.doi:10.1016/j.cemconres.2016.11.009
26. Cuesta A., Álvarez-Pinazo G., Sanfélix S. G., Peral I., Aranda M. A. G., & De la Torre A. G. (2014): Hydration mechanisms of two polymorphs of synthetic ye'elimite. *Cement and concrete Research, 63*, 127-136.doi:10.1016/j.cemconres.2014.05.010
27. Telesca A., Marroccoli M., Pace M. L., Tomasulo M., et al. (2014). A hydration study of various calcium sulfoaluminate cements. *Cement and Concrete Composites, 53*, 224-232. doi: 10.1016/j.cemconcomp.2014.07.002
28. Le Saoût G., Kocaba V., Scrivener K. (2011): Application of the Rietveld method to the analysis of anhydrous cement. *Cement and Concrete Research, 41*(2), 133-148. doi:10.1016/j.cemconres.2010.10.003
29. Guirado F., Galı S., Chinchón, S. (2000): Quantitative Rietveld analysis of aluminous cement clinker phases. *Cement and Concrete Research, 30*(7), 1023-1029. doi:10.1016/S0008-8846(00)00289-1
30. Bullerjahn F., Boehm-Courjault E., Zajac M., Haha M. B., Scrivener K. (2019): Hydration reactions and stages of clinker composed mainly of stoichiometric ye'elimite. *Cement and Concrete Research, 116*, 120-133.doi:10.1016/j.cemconres.2018.10.023
31. Bullerjahn F., Zajac M., Haha M. B., Scrivener K. L. (2019): Factors influencing the hydration kinetics of ye'elimite; effect of mayenite. *Cement and Concrete Research, 116,* 113-119.doi:10.1016/j.cemconres.2018.10.026
32. Shen Y., Qian J., Chai J., Fan Y. (2014): Calcium sulphoaluminate cements made with phosphogypsum: Production issues and material properties. *Cement and Concrete Composites, 48,* 67-74. doi:10.1016/j.cemconcomp.2014.01.009
33. Chen I. A., Juenger M. C. (2011): Synthesis and hydration

of calcium sulfoaluminate-belite cements with varied phase compositions. *Journal of Materials Science, 46*, 2568-2577. doi:10.1016/j.cemconcomp.2024.105714

34. Yan B., Ma L., Xie L., Ma J., Zi Z., Yan X. (2013): Reaction mechanism for iron catalyst in the process of phosphogypsum decomposition. *Industrial & Engineering Chemistry Research, 52*(49), 17383-17389. doi: 10.1021/ie402321w
35. Li X., Xu W., Wang S., Tang M., Shen X. (2014): Effect of SO_3 and MgO on Portland cement clinker: Formation of clinker phases and alite polymorphism. *Construction and Building Materials, 58*, 182-192. doi:10.1016/j.conbuildmat.2014.02.029
36. Li X., Zhang Y., Shen X., Wang Q., Pan Z. (2014): Kinetics of calcium sulfoaluminate formation from tricalcium aluminate, calcium sulfate and calcium oxide. *Cement and Concrete Research, 55,* 79-87. doi:10.1016/j.cemconres.2013.10.006
37. Bullerjahn F., Schmitt D., Haha M. B. (2014): Effect of raw mix design and of clinkering process on the formation and mineralogical composition of (ternesite) belite calcium sulphoaluminate ferrite clinker. *Cement and Concrete Research, 59*, 87-95. doi:10.1016/j.cemconres.2014.02.004
38. Sun Z., Nie S., Zhou J., Li H., et al. (2022): Hydration mechanism of calcium sulfoaluminate-activated supersulfated cement. *Journal of Cleaner Production, 333,* 130094.doi:10.1016/j.jclepro.2021.130094
39. Winnefeld F., Lothenbach B. (2010): Hydration of calcium sulfoaluminate cements—Experimental findings and thermodynamic modelling. *Cement and Concrete Research, 40*(8), 1239-1247. doi:10.1016/j.cemconres.2009.08.014
40. Martin L. H., Winnefeld F., Tschopp E., Müller C. J., Lothenbach B. (2017): Influence of fly ash on the hydration of calcium sulfoaluminate cement. *Cement and concrete research, 95,* 152-163. doi:10.1016/j.cemconres.2017.02.030
41. Shen Y., Chen X., Zhang W., Li X., Qian J. (2018): Influence of ternesite on the properties of calcium sulfoaluminate cements blended with fly ash. *Construction and Building Materials, 193,* 221-229. doi:10.1016/j.conbuildmat.2018.10.202
42. Chen D., Feng X., Long S. (1992): The structure and influence of ferric oxide on the properties of $3CaO{\cdot}3Al_2O_3{\cdot}BaSO_4$. *Thermochimica acta, 198*(2), 313-328. doi:10.1016/0040-6031(92)85088-D
43. Chen D., Feng X., Long S. (1993): The influence of ferric oxide on the properties of $3CaO{\cdot}3Al_2O_3{\cdot}CaSO_4$. *Thermochimica Acta, 215*, 157-169.doi:10.1016/0040-6031(93)80088-R
44. Benarchid M. Y., Rogez J. (2005): The effect of Cr_2O_3 and P_2O_5 additions on the phase transformations during the formation of calcium sulfoaluminate C_4A_3S. *Cement and Concrete Research, 35*(11), 2074-2080. doi: 10.1016/j.cemconres.2005.06.005
45. Winnefeld F., Barlag S. (2010): Calorimetric and thermogravimetric study on the influence of calcium sulfate on the hydration of ye'elimite. *Journal of Thermal Analysis and Calorimetry, 101*(3), 949-957.doi: 10.1007/s10973-009-0582-6
46. Cuesta A., Álvarez-Pinazo G., Sanfélix S. G., Peral I., et al. (2014): Hydration mechanisms of two polymorphs of synthetic ye'elimite. *Cement and Concrete Research, 63,* 127-136. doi:10.1016/j.cemconres.2014.05.010
47. Chen L., Wang X., Shen X. D., Ma S. H., Zhou W. Q. (2014): Crystal structure and hydration characteristics of tricalcium silicate doped with magnesium oxide. *Advanced Materials Research, 936*, 1336-1341. doi:10.1016/j.tca.2008.03.013
48. Thompson R. A., Killoh D. C., Forrester J. A. (1975): Crystal Chemistry and Reactivity of the MgO-Stabilized Alites. *Journal of the American Ceramic Society, 58*(1-2), 54-57.doi: 10.1111/j.1151-2916.1975.tb18984.x
49. Pelletier-Chaignat L., Winnefeld F., Lothenbach B., Le Saout G., Müller C. J., Famy C. (2011): Influence of the calcium sulphate source on the hydration mechanism of Portland cement–calcium sulphoaluminate clinker–calcium sulphate binders. *Cement and Concrete Composites, 33*(5), 551-561.doi:10.1016/j.cemconcomp.2011.03.005
50. Haha M. B., Winnefeld F., Pisch A. (2019): Advances in understanding ye'elimite-rich cements. *Cement and Concrete Research, 123,* 105778. doi:10.1016/j.cemconres.2019.105778
51. Zajac M., Skocek J., Bullerjahn F., Lothenbach B., Scrivener K., Haha M. B. (2019): Early hydration of ye'elimite: Insights from thermodynamic modelling. *Cement and Concrete Research, 120*, 152-163.doi:10.1016/j.cemconres.2019.03.024
52. Hargis C. W., Telesca A., Monteiro P. J. (2014): Calcium sulfoaluminate (Ye'elimite) hydration in the presence of gypsum, calcite, and vaterite. *Cement and Concrete Research, 65*, 15-20.doi:10.1016/j.cemconres.2014.07.004
53. Winnefeld F., Lothenbach B. (2010): Hydration of calcium sulfoaluminate cements—Experimental findings and thermodynamic modelling. *Cement and Concrete Research, 40*(8), 1239-1247.doi:10.1016/j.cemconres.2009.08.014